Effects of fuel compositions on the heat generation and emission of syngas/producer gas laminar diffusion flame

Tananop Piemsinlapakunchon and Manosh C. Paul*

Systems, Power & Energy Research Division, School of Engineering, University of Glasgow, Glasgow, G12 8QQ, United Kingdom

*Corresponding author: Email: Manosh.Paul@glasgow.ac.uk

Tel: +44 (0)141 330 8466

Abstract

Demand for the clean and sustainable energy encourages the research and development in the efficient production and utilisation of syngas for low-carbon power and heating/cooling applications. However, diversity in the chemical composition of syngas, resulting due to its flexible production process and feedstock, often poses a significant challenge for the design and operation of an effective combustion system. To address this, the research presented in this paper is particularly focused on an in-depth understanding of the heat generation and emission formation of syngas/producer gas flames with an effect of the fuel compositions. The heat generated by flame not only depends on the flame temperature but also on the chemistry heat release of fuel and flame dimension. The study reports that the syngas/producer gas with a low H_2:CO maximises the heat generation, nevertheless the higher emission rate of CO_2 is inevitable. The generated heat flux at H_2:CO = 3:1, 1:1, and 1:3 is found to be 222, 432 and 538 Wm^{-2} respectively. At the same amount of heat generated, H_2 concentration in fuel dominates the emission of NO_x. The addition of CH_4 into the syngas/producer gas with H_2:CO = 1:1 also increases the heat generation significantly (e.g. 614 Wm^{-2} at 20%) while decreases the emission formation. In contrast, adding 20% CO_2 and N_2 to the syngas/producer gas composition reduces the heat generation from 432 Wm^{-2} to 364 and 290 Wm^{-2}, respectively. The role of CO_2 on this aspect, which is weaker than N_2, thus suggests CO_2 is preferable than N_2. Along with the study, the significant role of CO_2 on the radiation of heat and the reduction of emission are examined.

Keywords: Syngas/producer gas; Syngas combustion; Laminar diffusion flame; Combustion modelling; Heat generation; Emission

1 Introduction

Among the various clean and sustainable sources of energy, the gas mixture fuel containing primarily hydrogen (H_2) and carbon monoxide (CO) namely 'syngas' is one of the interesting options. The advantage is the flexibility in its production process (e.g. through gasification, pyrolysis etc.) from various feedstocks (e.g. biomass, coal, waste) [1], [2], [3], [4], and [5]. However, an unavoidable side effect of this advantage arises with the variation of the chemical composition of product syngas or producer gas. The fuel composition contains not only H_2 and CO but also Nitrogen (N_2), steam (H_2O), carbon dioxide (CO_2) and methane (CH_4) at different volume fraction, depending on their production processes and feedstocks. As this fuel has the potential to replace conventional carbon fuel [6] and [7], an in-depth understanding of the heat generation and emission from combustion of this fuel is essential. This will hence guide the effective utilisation of this fuel in combustion system as well as the production of syngas/producer gas, with a higher concentration of desirable species, to potentially increase the heat generation but with low emission.

Recent research on the combustion of syngas/producer gas was primarily focused on the chemistry mechanisms which explained the combustion processes of syngas and their characteristics. Both the experimental and numerical methods were employed as an investigation tool. For example, the chemistry reaction mechanisms such as GRI3 [8], DRM22 [9], and Heghes' C_1–C_4 [10] were assessed by Fisher and Jiang [11] with the aim of finding the most suitable chemistry mechanisms for predicting the combustion of syngas/producer gas. Good prediction, in terms of the ignition delay time, was obtained with the numerical computation based on these three mechanisms when compared to the experimental result.

The GRI3 mechanism has an additional advantage of including the formation of Oxides of Nitrogen (NO_x). The mechanism consists of the reaction pathway of both Nitric Oxide (NO) and Nitrogen Dioxide (NO_2). However, utilisation of this mechanism requires a longer computational time than the other mechanisms since a total of 53 species with 325 reactions are required to be calculated. Performance of GRI3 was also studied along with another 15 syngas combustion mechanisms in Olm et al. [12] where the ignition delay time, the flame velocity, and the concentration profile of producer syngas having various compositions were studied at a range of temperature, pressure, H_2:CO ratio, and equivalence ratio. The

numerical and experimental data were compared. This literature further demonstrated that the GRI3 mechanisms produced results which were analogous to the other 15 chemistry mechanisms.

As a mixture of combustible and non-combustible species, the energy density of syngas is significantly lower than that of a conventional gas fuel such as natural gas [13]. The combustion applications that are compatible with syngas are reviewed in [14]. Gas turbine and external combustion chamber are the interesting options for extracting energy from syngas as these applications do not require the high energy density fuel in the operation [13]. Nevertheless, the redesign of the combustion configuration is suggested in order to combust syngas effectively [15]. The combustion of fuel in these applications frequently relates to the formation of diffusion flame where the fuel and oxidizer are supplied into combustion separately.

Diffusion flame characteristics of syngas were also investigated in the several other works as per the literatures [16], [17], [18], [19], [20], [21], [22], [23] and [24]. Burner configuration selected for this purpose was either counter-flow or co-flow. Considering a counter-flow burner, the flammability limit along with the effect of diluents species on the flame behaviour of H_2/CO syngas was investigated by [16], [17], and [18]. The studies based on the counter-flow burner revealed the role of H_2 on an increase of the flame temperature as well as NO_x emission. Conversely, the concentration of H_2O, CO_2 and N_2 in syngas fuel composition was found to reduce the flame temperature. The flame formulated by a co-flow burner is utilised in several practical combustion applications (such as those can be found in industrial furnace and cooking hob), and the flame of syngas/producer gas was studied at some extend by [19], [20], [21], [22], [23] and [24]. These studies particularly focused on the effects of each species in the fuel composition of syngas/producer gas in terms of the flame characteristics e.g. flame temperature, flame height, and emission formation rate.

The knowledge gap on the generation and utilisation of heat from the co-flow flames still remains unknown. The heat generation capability of a flame is affected by not only the temperature and structure of flame but also with the various additional factors related to the flame size, chemistry reaction, and gas medium around the flame. Therefore, it is anticipated that the impact of diversity in the fuel composition on these aspects would subsequently affect the heat generation property of the flame. Once this crucial fact is known, it will be potentially beneficial for the utilisation of syngas/producer gases in a practical combustion

system, and also for the development of syngas/producer gases with a high concentration of preferable species. Furthermore, the configuration of the co-flow burner is the fundamental of all the non-premixed combustion systems e.g. gas turbine combustor. Thus, the information obtained from this flame type could potentially be a guideline for predicting the heat generation in such a system as well.

Therefore, in light of the above literature review and the knowledge gap identified, the key objective sets for this study is to investigate the impacts of the fuel composition of syngas/producer gas on the heat generation, as well as on the emission formation of both CO_2 and NO_x. The study firstly focuses on the flame characteristics, considering the flame temperature and the flame surface area. The role of the flame characteristics on the heat generation capability is secondly examined. Lastly, the emission formation is studied based on the perception that it is a price to pay for a certain amount of heat generated. Computational fluid dynamics (CFD) model of a co-flow burner is developed for this purpose with a finite rate chemistry model selected for computing the detailed combustion reactions. The full GRI 3.0 reaction mechanism is utilised for the reaction pathway, with the thermodynamics and transport properties of related species. The model is coupled with thermal radiation in a participating media, in which the radiation transport is solved by discrete ordinary method (DOM). Thermal diffusion and multi-component diffusion are also selected (Warnatz model [25]) for defining the diffusive flux.

2 Burner configuration and numerical method

The selected co-flow burner is the same as the one presented in Toro et al. [26] and the appearance of this burner including its configuration is shown in Figure 1. The inner diameter of the fuel inlet tube is 9 mm with the tube thickness of 1 mm, whereas the inner diameter of the co-flow air intake is 95 mm. The fuel inlet is positioned 8 mm above the co-flow air inlet with the velocity profile of fuel injection considered to be parabolic, while a bulk profile is selected for the co-flow air. Both the streams, however, are supplied into the combustion chamber at the same average velocity and temperature of 0.5 ms^{-1} and 298 K respectively. The total pressure where the combustion occurs is 101325 Pa.

The burner was initially modelled for studying the characteristics of laminar diffusion H_2/N_2 flame in Piemsinlapakunchon and Paul [27]. However, some modifications are made to this model. E.g. the domain length is extended from 20.8 to 50.8 cm in order to support the

longer flame length of CH_4. This obviously results in an increase in the mesh cell number from 7800 to 17950 while keeping the same size of the smallest mesh cell. Details of the difference are reported in Table 1.

Boundary condition setup and the governing equations of continuity, momentum, energy, species transport and radiative transfer equations, and the material properties remain the same as those already presented in [27]. These governing equations are solved numerically in a segregated manner. The 'operator splitting' algorithm is selected for computing the species transport equation based on the supplied detailed chemistry reaction mechanism 'GRI3.0'. The radiative heat transfer is described by the discrete ordinate method (DOM) with gas mixture defined by the weighted sum of gray gases method (WSGGM) in which CO_2 and H_2O dominate the cloud emission and absorption among the other combustion gas products. Burner appearance, mesh generation, and boundary condition are also shown in Figure 1. Reliability of this model was already confirmed in [27] by having the good agreement of the numerical results of this model in all the test cases when compared to the experimental data of [26].

The model was also used for formulating the various flames at the same temperature, pressure, and flow velocity as presented in [27]. The fuel was ignited by setting the temperature of cells close to the fuel inlet at 1800 K for the first 1000 iterations. The simulation was then run until the contours of temperature, velocity, and distribution of major species (H_2, CO, H_2O, CO_2, N_2, NO and NO_2) became steady-state with the residuals of the converged solutions of the continuity, momentum, and energy equations staying between 10^{-3} and 10^{-6}. Further details on the numerical approach utilised in the study were given in [27] and will not be repeated here.

3 Flame modelling and case setup

Total 15 co-flow diffusion flames with a variation in the fuel composition of H_2, CO, CH_4, CO_2, and N_2 are formulated through the generated CFD model. The details about the fuel composition of these flames are shown in Table 2. They could be divided into 4 categories as follows:

(i) Single species fuel e.g. H_2 or CH_4.

(ii) Syngas with a H_2:CO concentration ratio of 1:3, 1:1, and 3:1

(iii) Syngas with H_2:CO = 1:1 and mixed with CH_4, CO_2, or N_2.

(iv) Producer gases produced from bamboo, rubber wood, wood pellets, and rice husk [2], [3], [28], [29], and [30], respectively.

The simulation result of H_2 and CH_4 flames which are conventional is utilised as a reference. By comparing their results with the result of syngas/producer gas, the effect of having H_2 and CH_4 in the fuel composition on each aspect could be explained. The fuel composition of flames in category (ii) is set to illustrate the impact of H_2 and CO concentration. The syngas with a H_2:CO concentration ratio of 1:3, 1:1, and 3:1 is represented by CO-rich, EQ, and H_2-rich respectively. The effect of adding CH_4, CO_2, or N_2 into the fuel composition of syngas is projected by the analysis of flames in category (iii). The flames in this category are represented by EQ+n%CH_4, EQ+n%CO, and EQ+n%N_2; where n gives the number of percentage. The flames in category (iv) are formulated from various biomass producer gases which are chosen from different sources. The study of flame in this category projects the heat generation capability of practical producer gas compared to the ideal syngas (category (ii)) and conventional fuel (category (i)).

4 Results and discussion

4.1 Heat generation

The diversity in the fuel composition of syngas/producer gas plays a significant role in the flame characteristics [19] and [31]. The different concentration ratio of species H_2, CO, CH_4, CO_2 and N_2 in the fuel composition of syngas/producer gas affects the flame temperature, dimension and chemistry heat release rate. These aspects of flame characteristics directly affect the heat generation capability of the flame. The temperature contour plot of each flame is initially analysed as presented in Figure 2. The difference in temperature and dimension between the different flames is illustrated. The flame front line is drawn to project the stoichiometric contour and dimension of the flame. On this line, the combustion of fuel and oxidizer occurs at the stoichiometric condition. The flame front line is plotted by the zero-temperature gradient method. This method considers the grids, with the highest temperature at each vertical and horizontal level in the grid system, as a position where the stoichiometric combustion condition takes place. These grids have the temperature gradient as zero and the connection between them forms the stoichiometric contour called ‘flame front line’.

The flame temperature and dimension are extracted from the temperature contour and compared in Figure 3 and Figure 4 respectively. In this analysis, the flame temperature (T) is the maximum temperature on the temperature contour. The flame front lines of all the studied flames are plotted together to illustrate their differences in dimension. To compare the size, the flame surface area (A_f) is computed by integrating the flame front line around the domain axis as presented in Figure 3. This parameter refers to the size of the stoichiometric contour of the flame; thus, it represents the size of the flame as well as the size of the reaction zone. The diversity in fuel composition of the studied flames causes the difference in their reaction pathways and subsequently, results in the different heat release rate from the related chemical reactions. The analysis of chemistry heat release is processed at two layers. The first one is the chemistry heat release property of fuel where the parameter representing this aspect is the maximum chemistry heat release on the contour plot (Q_{max}). This parameter expresses the highest possible chemistry heat release property of the specific fuel. It therefore provides with the understanding of fuel combustion property which is typically analysed based on the concentration percentage of fuel species H_2, CH_4, and CO through other parameters such as the lower heating value (LHV) and higher heating value (HHV). The second layer is the total chemistry heat release generated by flame (Q_{total}). This is processed by combining the chemistry heat release rate at every grid on the simulation domain. To simplify, the chemistry heat release property of fuel is represented by Q_{max} while the total chemistry heat release of a flame is expressed by Q_{total}. The comparison of these parameters of all the studied flames is presented in Figure 5.

In category (i), the value of T and Q_{max} obtained from the H_2 flame (2297 K and 0.25 W) is higher than one computed from the CH_4 flame (2016 K and 0.22 W). The H_2 gas fuel thus releases more heat from its chemistry reaction during combustion than CH_4. On the other hand, the dimension of CH_4 flame is wider and significantly longer than those of the H_2 flame. This obviously leads to the larger A_f for the CH_4 flame (8.35E-3 m^2) than the H_2 flame (1.35E-3 m^2). Further, the meaningfully larger A_f of CH_4 flame refers to its larger reaction zone which consequently results in the higher value of Q_{total} (1058 W) although its Q_{max} is lower than that of the H_2 flame which generates Q_{total} as 357 W. According to this, the heat release property of fuel (Q_{max}) is not the only factor affecting the heat generation of flame. The size of the flame also plays a significant role and the larger one could compensate with the lower Q_{max}. Furthermore, the analysis of flame in this category, which contains single species, could be used as a guideline in the analysis of the flames in the other categories.

The effect of H_2:CO concentration ratio is projected in the analysis of flames in category (ii). The result of H_2 flame (category (i)) supports the direction of the result. The combustion of syngas with the higher concentration ratio of H_2:CO releases heat at a higher rate (higher Q_{max}) also the higher values of T is predicted from the flame of this fuel. As seen, the highest values of T and Q_{max} are computed from the H_2-rich syngas (2228 K and 0.22) followed by the EQ (2169 K and 0.19 W) and CO-rich syngas (2109 K and 0.15 W). Comparing the dimension, the flame of syngas with a higher H_2:CO is shorter but wider than the syngas having a higher ratio. The comparison of flame size based only on the flame length might not be suitable in this case since the flame with wider width could have a larger size than a longer flame. This, therefore, requires the analysis of flame surface area to further examine the effect of H_2:CO on the flame size and reaction zone. The result observed for A_f for the flame of CO-rich (1.55E-3 m^2) syngas is larger than EQ (1.47E-3 m^2) and H_2-rich syngas (1.39E-3 m^2). Hence, A_f of the syngas flame with a lower H_2:CO is larger and the role of CO on the escalation of flame size is confirmed. The combustion of syngas with the lower H_2:CO releases less heat (i.e. lower Q_{max}); however, the flame of this fuel has the larger size which compensates the lower Q_{max} and results in the higher flame total heat release (higher Q_{total}). As seen, the highest Q_{total} in this category is found from the CO-rich syngas (363 W) followed by the EQ (355 W) and H_2-rich syngas (350 W).

Species CH_4, CO_2, or N_2 are added into the fuel composition of EQ syngas gas at 10% and 20% in category (iii). The simulation result of CH_4 flame in category (i) is used as a guideline in the analysis. Comparing the flame of CH_4 with one of the EQ syngas, it is found that the CH_4 flame has lower T but higher A_f, Q_{max}, and Q_{total}. For example, the flame temperature of EQ syngas mixed with CH_4 reduces to 2130 and 2108 K at 10% and 20% of addition respectively. Conversely, the flame size increases to 2.04E-3 m^2 and 2.64E-3 m^2 for 10% and 20% of additional percentage. The combustion of EQ syngas mixed with CH_4 releases slightly higher heat (Q_{max} = 0.195 W for EQ+20%CH_4) than EQ syngas when the additional percentage is 20%. As the parameters, A_f and Q_{max}, are escalated by the addition of CH_4, the higher value of Q_{total} is generated by the flame of EQ+20%CH_4 (495 W) followed by EQ+10%CH_4 (425 W) and EQ syngas.

Furthermore, adding CO_2 and N_2 to syngas/producer gas decreases the total percentage of fuel species and the lower T, A_f, Q_{max}, and Q_{total} are expected. The comparison of flames in category (iii) where 10% and 20% of either CO_2 or N_2 is added to EQ syngas projects the

effect of this action. Specifically, at 10%, the value of T and A_f decreases to 2090 K and 1.41E-3 m^2 respectively for the addition of CO_2, and 2124 K and 1.36E-3 m^2 for the addition of N_2. The trend also continues at the additional percentage of 20%. E.g. EQ+20%CO_2 has the flame temperature and size as 2001 K and 1.35E-3 m^2 respectively while the value of T and A_f of EQ+20%N_2 are 2070 K and 1.25E-3 m^2. Moreover, as seen, the dilution of syngas at the same percentage of CO_2 and N_2 affects the reduction of T and A_f at different levels. Therefore, not only the fuel species (H_2, CO and CH_4) but also the diluted species CO_2 and N_2 affect the value of T and A_f. According to the results, CO_2 has a stronger effect on the decrease in flame temperature and N_2 has a stronger effect on the reduction of flame size. Regarding the chemistry heat release, the addition of either CO_2 or N_2 decreases the value of both Q_{max} and Q_{total}. the higher percentage of addition leads to the lower value since the percentage of fuel species is lower. At the same additional percentage, it is found that the value of Q_{max} and Q_{total} of EQ syngas mixed with CO_2 is almost equal to one mixed with N_2. For example, Q_{max} of EQ+10%CO_2 and EQ+10%N_2 is 0.17 W while Q_{total} of these fuels is 319 W. At 20% of additional percentage, EQ syngas mixed with either CO_2 or N_2 has Q_{max} and Q_{total} of 0.16 W and 283 W respectively. According to this, the effect of CO_2 and N_2 on the chemistry heat release are considered as comparable and insignificant comparing to the role of fuel species.

The impact of diversity in fuel composition obtained from the study of flames in category (ii) and (iii) is applied for explaining the characteristics and heat generation of flames of producer gases in category (iv). The highest flame temperature in this category is computed from the flame of producer gas produced from wood pellets (1746 K) which contains the highest total percentage of fuel species (44.4%) and the highest H_2:CO ratio (1.04). Conversely, the lowest flame temperature is predicted from the flame of rubberwood producer gas (1674 K) which has the lowest H_2:CO ratio (0.86) also total fuel species percentage (39.4%). The dimension of flames in this category is compared and the flame size is computed between 9.5E-4 m^2 and 1.0E-3 m^2. The role of total fuel species concentration percentage is confirmed since the combustion reaction of producer gas of wood pellets generates heat at the highest rate (Q_{max} = 0.11 W). Also, the flame of this fuel generates the highest heat as 174 W of Q_{total}. The opposite direction of the result is computed from producer gas of rubberwood (Q_{max} = 0.099 W and Q_{total} = 150 W).

4.2 Heat transfer

The analysis of heat transferred from flame could be processed by the thermal radiation model selected. This model is capable of computing the heat radiated through the participating media in which the high-temperature combustion product gases e.g. H_2O and CO_2 play a key role in emission and absorption of heat. The diversity in fuel composition of syngas/producer gas causes the different production rate of these product gases due to different reaction pathways and concentration of fuel species as a reactant of the chemistry reaction. This, consequently, affects the heat transfer capability of the flame. To examine this, heat flux is measured on the left boundary of the simulation domain (left-hand outlet boundary in Figure 1) for all the studied flames. The heat flux profile is compared as shown in Figure 6.

In category (i), the profile of CH_4 is outstanding from the other fuels. It begins with the heat flux of 554 W-m^{-2} at zero vertical distance then increases significantly to the peak value at 1781 W-m^{-2} at 0.17 m of the vertical distance. Above this level, the heat flux reduces dramatically until passing the top boundary of the domain. The difference in the profile pattern is seen from the heat flux profile of H_2 flame since two peaks are observed. The profile of H_2 is 672 W-m^{-2} at zero vertical distance and rises to the first peak value (948 W-m^{-2}) at 0.02 m then it slightly decreases and increases again to the second peak (960 W-m^{-2}) at 0.05 m in vertical distance. Beyond this position, the heat flux profile of H_2 flame has a downtrend. Due to this, the pattern of the heat flux profile is affected differently by different fuel species. The position of the highest peak (the second peak for H_2 flame.) depends on the flame length.

The effect of having H_2 in fuel composition could be seen from the heat flux profile of flames in category (ii). As seen, the profile of H_2-rich syngas has two peaks similar to the profile of H_2 flame. However, the first peak of the heat flux profile of H_2-rich syngas (895 W-m^{-2} at 0.015 m) is clearly lower than the second peak (1018 W-m^{-2} at 0.055 m). The concentration percentage of H_2 in fuel composition affects the value of the first peak, and the lower percentage of H_2 causes the first peak value lower and disappears as seen from the heat flux profile of EQ and CO-rich syngas. As a result, the second peak of the heat flux profile is the maximum heat flux of flames in this category. This maximum value relates to the concentration of CO and the flames of syngas having the higher CO concentration radiates the heat flux with the higher maximum value. Furthermore, the effect of flame length on the

position of the maximum heat flux (the second peak) is in the same direction for flames in both categoris (i) and (ii); the longer flame length causes the higher position of the peak. The highest maximum heat flux in this category is computed from CO-rich syngas (1518 W-m^{-2} at 0.065 m) followed by EQ syngas (1309 W-m^{-2} at 0.058 m) and H_2-rich syngas.

Focusing the heat flux profile of flames in category (iii), the pattern is similar to EQ syngas in category (ii) since the H_2:CO is the same as 1. The first peak is unclear due to the concentration of H_2 and CO which are 40-45%. The heat flux profile of EQ syngas mixed with CH_4 is in the same direction as one of the CH_4 flame. The concentration percentage of CH_4 plays a significant role on the heat flux; for example, the peak value of heat flux profile of EQ+20%CH_4 (1503 W-m^{-2} at 0.085 m) is higher than that of EQ+10%CH_4 (1404 W-m^{-2} at 0.07 m). The level of effect of CO and CH_4 increasing the maximum heat flux could be examined through the comparison of the heat flux profile between the EQ syngas, EQ+10%CH_4, and EQ+20%CH_4. Both CO and CH_4 have a strong effect on an increase in the maximum heat flux. Additionally, the role of CH_4 is stronger than CO on this aspect.

To understand the role of CO_2 and N_2 on heat flux, the heat flux profile of EQ syngas is used as a reference and compared with EQ syngas mixed with either CO_2 or N_2. The maximum heat flux is lower when either of these species is added into fuel composition. The lower total percentage of fuel species also plays a key role in the profile of heat flux especially when the H_2:CO ratio close to 1. It is noticed that the level of effect of CO_2 and N_2 on the heat flux profile is different. As seen, EQ+10%CO_2 (1245 W-m^{-2} at 0.0593 m) is higher than EQ+10%N_2 (1125 W-m^{-2} at 0.0579 m), and EQ+20%CO_2 (1155 W-m^{-2} at 0.0603 m) is also higher than EQ+20%N_2 (936 W-m^{-2} at 0.0568 m). This finding relates to having a significant role of CO_2 on the thermal radiation. For instance, the numerical model for computing thermal radiation (WSGG model) considers this species to dominate the cloud emission and absorption of heat radiation. According to the result obtained, having this species in the fuel composition reduces the flame temperature significantly but increases the radiation of heat flame. On the other hand, the position of the peak heat flux is confirmed to be strongly affected by the flame length; and the longer flame also has the higher position of maximum heat flux.

The result predicted from the flames in category (iv) supports the finding from the other categories. The heat flux profile of them relies on the fuel composition and the flame length. The lower percentages of CO (20.4 – 22.6%) and CH_4 (1.4 - 2.2%) in the fuel composition of

flames in this category are significantly lower than the fuels in the other categories. As a result, the first and second peaks of the heat flux profile are clearly observed. The flame length in this category is also comparable; hence, the position of the maximum heat flux (the second peak of the profile) is similar (~0.057 m). Further, as the ratio of H_2:CO is close to 1, the flame having a higher total percentage of fuel species has a higher maximum heat flux. In case that the percentage is similar, one with a higher percentage of CO and CH_4 has a higher peak value. As seen, the highest maximum heat flux is computed from the producer gas of rice husk (492 W-m^{-2}) followed by one of wood pellets (480 W-m^{-2}), bamboo (430 W-m^{-2}), and rubber wood (384 W-m^{-2}).

The study of heat flux profile projects the information of generated heat at each vertical distance from the co-flow air exit. This provides the guideline for effectively utilising these flames as a source of energy. However, the comparison of heat flux of different flames based on their heat flux profile could be difficult. The complex pattern of heat flux profile could cause confusion. To address this, the average heat flux ($Q´$) is calculated from the heat flux profile and the area of the measured boundary. The comparison between the average heat flux ($Q´$) of all studied flames is presented in Figure 7. This parameter illustrates the different capability of various flames for the generation of heat flux. The highest $Q´$ among the studied flames is outstandingly provided by the flame of CH_4 (1293 W-m^{-2}). Analysing $Q´$ of the flames within the same category, the result is in the same direction for the effect of fuel composition on the maximum value of the heat flux profile. The comparison of $Q´$ also allows the cross comparison between flames in different categories. This points to the interesting result since the flames with the lower total percentage of fuel species (80-90%) could generate a higher $Q´$ than ones with 100% total fuel species. As seen, $Q´$ of EQ+10%N_2 (360 W-m^{-2}), EQ+10%CO_2 (403 W-m^{-2}), EQ+20%N_2 (290 W-m^{-2}), and EQ+20%CO_2 (364 W-m^{-2}) are higher than $Q´$ of H_2 (222 W-m^{-2}) and H_2-rich syngas (280 W-m^{-2}). This result further emphasizes the role of carbon fuel species and CO_2 on the heat flux generation and heat transfer of flame. The flame of H_2 and H_2-rich with an absent and lower concentration of CO respectively cannot provide higher heat flux although their heat release from the chemistry reaction (Q_{total}) is higher.

4.3 Emission formation of CO_2 and NO_x

Combustion of gas fuel results in the emission formation of CO_2 and NO_x. These undesirable combustion products are a price to pay for the heat generation. By this

perception, the study of emission formation focuses on the production rate of CO_2 and NO_x based on the generated heat flux. The total production rate of them is firstly computed by combining their production rate on every grid of the simulation domain. For the production rate of NO_x, two species which are NO and NO_2 are considered. The calculation provides the total production rate of CO_2 and NO_x of each studied flames. Latterly, the emission formation rate per generated heat flux (CO_2 or NO_x production rate : Q') is calculated. This method considers the average heat flux (Q') presented in the previous section (Figure 7) as a heat generated and transferred by flame. The emission formation of CO_2 and NO_x is an inevitable side effect of heat generation by this perception. In other words, it illustrates the rate of emission formation that must be paid for 1 W-m^{-2} of generated heat flux. The comparison of CO_2 and NO_x production rate : Q' is presented in Figure 8.

At the same amount of heat generated from the flame, the study result shows that the flame of CH_4 formulates the lowest emission both CO_2 and NO_x. The ratio of CO_2 or NO_x production rate : Q' of this flame is lower due to its capability to generate heat flux at the highest rate among all studied flames. The reaction pathway of H_2 causes zero production rate of CO_2 from the flame of this fuel; nevertheless, the role of this species on an increase of flame temperature encourages the thermal NO_x formation and leads to the highest ratio of NO_x production rate : Q'. This finding also points to the impact of thermal NO_x formation mechanism which dominates the NO_x formation rate of flame having H_2 as a major fuel species. This direction of the result is supported by the result of flames in category (ii). The syngas flame having the higher H_2 in fuel composition has a higher flame temperature hence the higher ratio of NO_x production rate : Q'. On the other hand, the analysis of flame in category (i) and (ii) together provides the impact of carbon fuel species on the production rate of CO_2. The reaction pathways of both CH_4 and CO are the main source of the CO_2 production. The effect of CO is significantly stronger than CH_4 based on the same amount of heat flux generated. As seen, the CO_2 production rate : Q' of CO-rich is higher than one of CH_4 flame. As a result, the CO_2 emission rate per heat ratio of EQ syngas is improved when CH_4 is added to the fuel composition as seen from the result predicted from the flames of EQ+10%CH_4 and EQ+20%CH_4.

The lower total percentage of fuel species of syngas consisting N_2 in fuel composition (EQ syngas mixed with N_2) causes the lower total CO_2 and NO_x production rate computed from flame comparing to EQ syngas. Conversely, the heat flux generated by these flames is

also lower. As a result, the ratio of CO_2 production rate : $Q´$ is higher than EQ syngas. On the other hand, the ratio of NO_x production rate : $Q´$ of EQ syngas mixed with N_2 is lower. This emphasizes the role of H_2 and thermal NO_x formation since the concentration percentage of H_2 in EQ syngas mixed with N_2 is lower than EQ syngas. The significant role of CO_2 in fuel composition (as a reactant) on the thermal radiation mentioned in the previous section combines with the role of this species on the reduction of flame temperature causes the lower ratio of NO_x production rate : $Q´$. Having this species in fuel composition (as a reactant) is also found to decrease the total CO_2 production rate (as a product). The lower CO_2 production rate : $Q´$ of EQ syngas mixed with CO_2 could be seen from the comparison between EQ syngas, EQ+10%CO_2, and EQ+20%CO_2.

Lastly, the flames of producer gas in category (iv) have significantly lower flame temperature and total fuel species than flames in the other categories. Their total production rate of CO_2 is lower due to the concentration percentage of CO and CH_4. However, the value of $Q´$ of flames in this category is also significantly lower than the others. Combining these factors, the CO_2 production rate : $Q´$ of the flames in this category is higher than flames in the other categories. Almost double CO_2 formation is predicted for the same amount of heat generation comparing to the flame of pure syngas (category ii). The concentration of CO and CH_4 of each flame in this category is comparable. This leads to a similar total production rate of CO_2. Within category (iv), the ratio of CO_2 production rate : $Q´$ is hence dominated by the heat flux generated and the flame formulating the higher $Q´$ has the lower ratio. On the other hand, the meaningfully lower flame temperature of producer gas causes the lower total NO_x production rate computed. The ratio of NO_x production rate : $Q´$ of producer gas flame is, therefore, lower than one of the flames in category (ii). Within category (iv), the flame having a higher flame temperature also produces the higher NO_x production rate : $Q´$.

5 Discussion

The results presented in the previous sections provided an understanding of the heat generation and emission of syngas/producer gas especially with the effect of fuel composition. The key finding is analysed and discussed together in this section as follows:

The flame with high temperature is expected to increase heat transfer; nevertheless, the result shows that the flame dimension, surface area (A_f) and chemistry heat release of fuel (Q_{max}) are also the key parameters which affect the chemistry heat release of flame (Q_{total})

and consequently, the average heat flux ($Q´$). Analysing the relationship between the flame temperature and Q_{max}, the flame having a higher flame temperature also has a higher value of Q_{max}. This condition is valid for the comparison of flame within the same category but not for any cross-category comparison. As the fuel composition in each category is defined to project the effect of fuel composition, the effect of species H_2, CO, CH_4, CO_2, and N_2 on Q_{max} is in the same direction as the flame temperature. However, it does not mean that the flame having a higher flame temperature could generate higher Q_{max}. For example, the flame temperature of CO-rich syngas is higher than EQ-syngas+20%CO_2 but the value of Q_{max} of the previous fuel is lower.

Flame dimension also plays a significant role on both the heat generation and heat transfer. Firstly, longer and wider dimension lead to larger flame surface area (A_f) which could compensate for the lower chemistry heat release of fuel (Q_{max}) with higher Q_{total}. Secondly, longer flame length extends the position of the maximum heat flux. This further creates a larger area on the boundary such that the flame could radiate heat flux at a higher rate, which leads to the higher average heat flux ($Q´$). As a result, the heat generation and heat transfer of flame could be improved by extending the width and length of the flame. This could be processed by the development of fuel composition to increase the concentration of species that provides the larger flame size. Also, an increase in fuel velocity is another option. Nevertheless, this method increases the opportunity that the flame could become unstable and transforms the flow regime from laminar to turbulent.

Furthermore, the analysis provides the guideline for the development of fuel composition. Three fuel species H_2, CO, and CH_4 provide the heat generation and heat transfer at a different level. The fuel composition with the different ratio of them generates a different level of heat as seen from the results. The similar method as used for studying the emission formation rate could be used for roughly estimating the consumption of the studied fuels. For that, the velocity of fuel stream is converted to a volume flow rate and calculated per amount of average generated heat flux ($Q´$). As the velocity of all flames is equal, the consumption per heat flux is the indirect proportion to the value of $Q´$. The fuel that provides the lower $Q´$ requires a higher fuel consumption. Due to this, CH_4 is the most preferable species since it provides a significant higher heat with the lower emission rate and consumption. In case that the heat generation and fuel consumption are prioritised, rising the CO concentration percentage in the fuel composition is the solution but the significantly

higher CO_2 production rate is the side effect of this method. Alternatively, increasing H_2 in the fuel composition of syngas/producer gas reduces the CO_2 production rate; however, the higher fuel consumption and NO_x emission rate are expected.

The simulation result also reveals the benefit of adding CO_2 to the fuel composition on the values of $Q´$ and CO_2 production rate. Having CO_2 in fuel composition surprisingly provides the lower emission production rate per generated heat. In order to effectively utilise this species, further study such as the impact of injecting CO_2 along with the fuel and air streams to combustion is suggested.

Finally, with regards to the other studies in the literature, the role of each species in the fuel composition presented on the flame temperature appears to have the same trend as reported in [16], [17], and [21]. That is, H_2 content in syngas has a stronger effect than CO on the increase of flame temperature. The role of H_2 and CO on the flame temperature is also considered to be well comparable with the study of [19], but the impact of H_2:CO seems to be minor. This could be due to the fact that the flow regime of fuel stream which is laminar for our work, while it was turbulent in [19]. Further, in terms of the flame dimension and NO_x emission, the results obtained in this work also have the same trend as reported in [21] and [24].

6 Conclusion

Heat generation and emission of conventional fuel, and syngas/producer gas are investigated with a finite rate chemistry model combining the GRI3 chemistry mechanisms. The key conclusions from the study are drawn as explained in the bullet points below:

- An estimation of heat generation from the studied fuels would consider not only flame temperature but also fuel combustion heat release (Q_{max}) and flame dimension. Both parameters play a significant role and could compensate for the role of each other. The fuel providing the lower Q_{max} could formulate the flame with the higher Q_{total} and $Q´$ if the flame has a larger dimension.

- CH_4 is the most preferable species in syngas/producer gas composition due to its capability on an increase of heat generation with a lower consumption and emission

formation rate per generated heat. CO is the second preferable one in terms of heat generation and fuel consumption. However, the significantly higher production rate of CO_2 per generated heat is inevitable. Lastly, a higher percentage of H_2 in fuel composition provides less heat generation but higher fuel consumption and NO_x production rate for the same amount of heat. Conversely, it could decrease CO_2 emission significantly.

- The significant role of CO_2 in fuel composition is pointed out for the radiation of heat and the reduction of emission. With the aim of effectively utilising this species, the further study on its impact and property is suggested.

Overall, comparing the performance of syngas and producer gas flames to the pure CH_4 flame in terms of the heat generation, it is found that the heat produced from the CH_4 flame is significantly higher. Two methods are recommended for an improvement of the heat generation: (i) developing fuel composition to release more heat and transfer it effectively, and (ii) increasing the fuel rate to escalate the dimension and surface area of the flame. The latter method would require further study since the instability and the transition of flow regime from laminar to turbulent could occur.

Acknowledgement

The first author would like to thank the Royal Thai Navy for funding his postgraduate research study at the University of Glasgow. The second author (M. C. Paul) acknowledges his RAEng/The Leverhulme Trust Senior Research Fellowship support (LTSRF1718\14\45) from the Royal Academy of Engineering, UK.

7 References

[1] P. Basu, Biomass Gasification, Pyrolysis, and Torrefaction Practical Design and Theory (second ed.), Amsterdam : Academic Press, 2013.

[2] A. M. Salem and M. C. Paul, "An integrated kinetic model for doendraft gasifier based on a novel approach that optimises the reduction zone of gasifier," *Biomass and Bioenergy,* vol. 109, pp. 172-181, 2018.

[3] A. M. Sepe, J. Li and M. C. Paul, “Assessing biomass steam gasification technologies using a multi-purpose model,” *Energy Conversion and Management,* vol. 129, pp. 216-226, 2016.

[4] A. M. Salem, U. Kumar, A. N. Izaharuddin, H. Dhami, T. Sutardi and M. C. Paul, “Advanced numerical methods for the assessment of integrated gasification and CHP generation technologies,” in *Coal and Biomass Gasification*, Singapore, Springer, 2018, pp. 307-330.

[5] T. Sutardi, M. C. Paul, N. Karimi and P. L. Younger, “Numerical Modelling for Process Investigation of a Single Coal Particle Combustion and Gasification,” in *World Congress on Engineering 2017 (WCE 2017)*, London, 2017, pp. 946-951.

[6] F. Lozano and R. Lozano, “Assessing the potential sustainability benefits of agricultural residues:Biomass conversion to syngas for energy generation or to chemicals,” *Journal of Cleaner Production,* vol. 172, pp. 4162-4169, 2018.

[7] J. D. Mackaluso, “The use of syngas derived from biomass and waste products,” *MMG 445 Basic Biotechnology eJournal ,* vol. 3, pp. 98-103, 2007.

[8] G. P. Smith, D. M. Golden, M. Frenklach, N. W. Moriarty, B. Eiteneer, M. Goldenberg, T. Bowman, R. K. Hanson, S. Song, W. C. Gardiner Jr., V. V. Lissianski and Z. Qin. [Online]. Available: http://www.me.berkeley.edu/gri_mech/. [Accessed 4 12 2017].

[9] A. Kazakov and M. Frenklach, “Reduced Reaction Sets based on GRI-Mech 1.2,” [Online]. Available: http://combustion.berkeley.edu/drm/. [Accessed 4 12 2017].

[10] C. I. Heghes, “C1-C4 Hydrocarbon Oxidation Mechanism,” [Online]. Available: http://www.ub.uni-heidelberg.de/archiv/7379. [Accessed 4 12 2014].

[11] M. Fischer and X. Jiang, “An assessment of chemical kinetics for bio-syngas combustion,” *Fuel,* vol. 137, pp. 293-305, 2014.

[12] C. Olm, . I. G. Zsély, . T. Varga, H. J. Curran and T. Turányi, “Comparison of the performance of several recent syngas combustion mechanisms,” *Combustion and Flame,* vol. 162, no. 5, pp. 1793-1812, 2015.

[13] L. Chanphavong and Z. A. Zainal, “Characterization and challenge of development of producer gas fuel combustor: A review,” *Journal of the Energy Institute,* pp. 1-14, 2018.

[14] A. Pradhan, P. Bareda and A. Kumar, “Syngas as An Alternative Fuel Used in Internal Combustion Engines: A Review,” *Journal of Pure and Applied Science & Technology,* vol. 5, no. 2, pp. 51-66, 2015.

[15] F. Delattin, G. Di Lorenzo, S. Rizzo, S. Bram and J. De Ruyck, “Combustion of syngas in a pressurized microturbine-like combustor: Experimental results,” *Applied Energy,* vol. 87, no. 4, pp. 1441-1452, 2010.

[16] J. Park, D. S. Bae, M. S. Cha, J. H. Yun, S. I. Keel, H. Chang Cho, T. K. Kim and J. S. Ha, “Flame characteristics in H2/CO synthetic gas diffusion flames diluted with CO2: Effects of radiative heat loss and mixture composition,” *International Journal of Hydrogen Energy,* vol. 33, no. 23, pp. 7256-7264, 2008.

[17] J. Park, O. B. Kwon, J. H. Yun, S. I. Keel, H. Chang Cho and S. Kim, “Preferential diffusion effects on flame characteristics in H2/CO syngas diffusion flames diluted with CO2,” *International*

Journal of Hydrogen Energy, vol. 33, no. 23, pp. 7286-7294, 2008.

[18] S. Hsin-Yi , H. Jou-Rong and L. Yu-Heng , "Computed flammability limits of opposed-jet H2/CO syngas diffusion flames," *International Journal of Hydrogen Energy,* vol. 39, no. 7, pp. 3459-3468, 2014.

[19] K. Ranga Dinesh, X. Jiang, M. Kirkpatrick and W. Malalasekera, "Combustion characteristics of H2/N2 and H2/CO syngas nonpremixed flames," *International Journal of Hydrogen Energy,* vol. 37, no. 21, pp. 16186-16200, 2012.

[20] P. Swarnkar, A. K. Sahu and T. Sundararajan, "Numerical study of effect of hydrogen content on the structure of syngas diffusion flame," in *10th International Conference on Heat Transfer, Fluid Mechanics and Thermodynamics*, Orlando, Florida, 2014, pp. 704-713.

[21] J. Xi, Y. Yuan, Z. Gu, W. Yang, X. Zhang and S. Wang, "Effect of CO2/N2/CH4 dilution on NO formation in laminar coflow syngas diffusion flames," *Energy sources,* vol. 40, no. 7, pp. 821-829, 2018.

[22] A. Cuoci, A. Frassoldati, G. Buzzi Ferraris, T. Faravelli and E. Ranzi, "The ignition, combustion and flame structure of carbon monoxide/hydrogen mixtures. Note 2: Fluid dynamics and kinetic aspects of syngas combustion," *International Journal of Hydrogen Energy,* vol. 32, no. 15 , pp. 3486-3500, 2007.

[23] L. Jeongwon, P. Sangwoon and K. Yongmo, "Effects of Fuel-Side Nitrogen Dilution on Structure and NOx Formation of Turbulent Syngas Non-premixed Jet Flames," *Energy fuels,* vol. 26, pp. 3304-3315, 2012.

[24] H. Xu, F. Liu, S. Sun, Y. Zhao, S. Meng and W. Tang, "Effects of H2O and CO2 diluted oxidizer on the structure and shape of laminar coflow syngas diffusion flames," *Combustion and Flame,* vol. 117, pp. 67-68, 2017.

[25] J. Warnatz, U. Maas and R. W. Dibble, Combustion: Physical and Chemical Fundamentals, Modeling and Simulations, Experiments, Pollutant Formation 3rd edition, Berlin Heidelberg: Springer-Verlag, 2001.

[26] V. V. Toro, A. V. Mokhov, H. B. Levinsky and M. D. Smooke, "Combined experimental and computational study of laminar, axisymmetric hydrogen–air diffusion flames," *Proceedings of the Combustion Institute,* vol. 30, no. 1, pp. 485-492, 2005.

[27] T. Piemsinlapakunchon and M. C. Paul, "Effects of content of hydrogen on the characteristics of co-flow laminar diffusion flame of hydrogen/nitrogen mixture in various flow conditions," *International Journal of Hydrogen Energy,* vol. 43, no. 5, pp. 3015-3033, 2018.

[28] G. M. Vincent, "Key Combustion Issues Associated with Syngas and High-Hydrogen Fuels," University of California Irvine, 2006.

[29] T. Sutardi, M. C. Paul and N. Karimi , "Investigation of Coal Particle Gasification Processes with Application Leading to Underground Coal Gasification," *Fuel,* vol. 237, p. 1186–1202, 2019.

[30] U. Kumar and M. C. Paul, "CFD modelling of biomass gasification with a volatile break-up approach," *Chemical Engineering Science,* vol. 195, pp. 413-422, 2019.

[31] T. Piemsinlapakunchon and M. C. Paul, “Characterisation of Syngas Laminar Diffusion Flame with an Effect of its Varying Composition,” in *World Congress on Engineering 2017, pp1008-1012, ISBN 9789881404831*, London, UK, 2017.

[32] C. T. Bowman, R. K. Hanson, D. F. Davidson, W. C. Gardiner, V. Lissianski, G. P. Smith, D. M. Golden, M. Frenklach and M. Goldenberg, “GRI-Mech,” 2008. [Online]. Available: http://www.me.berkeley. edu/gri-mech/. [Accessed 31 May 2017].

Table 1 Details of the mesh generation used for the mesh dependency test

Literature	Levels from the outer of the fuel outlet tube to the axis	Levels from the outer of the fuel outlet tube to the top plane	Levels from the outer of the fuel outlet tube to the left plane	Levels from the outer of the fuel outlet tube to the top plane	Total number of cells	Smallest cell size (mm)
Piemsinlapakunchon and Paul [27]	16	100	50	24	7800	0.2
This work	16	250	50	24	17950	0.2

Table 2 Details of the studied fuel compositions

Flame	H_2	CO	CH_4	CO_2	N_2	Total fuel % (H_2, CO, and CH_4)	H_2:CO	Density (kg-m^{-3})	Mass flow rate (x 10^{-5} kg-s^{-1})	Volume flow rate (x 10^{-5} m^3-s^{-1})	Air–fuel ratio	Lower heating value (MJ/kg)
H_2	100.0%	-	-	-	-	100.0%	-	0.082	0.26	3.21	2.38	141.58
CH_4	-	-	100.0%	-	-	100.0%	-	0.656	2.10	3.21	9.52	55.51
H_2-rich	75.0%	25.0%	-	-	-	100.0%	3	0.348	1.17	3.21	2.38	33.30
EQ	50.0%	50.0%	-	-	-	100.0%	1	0.614	1.97	3.21	2.38	18.86
CO-rich	25.0%	75.0%	-	-	-	100.0%	0.33	0.878	2.82	3.21	2.38	13.15
EQ+10%CH_4	45.0%	45.0%	10.0%	-	-	100.0%	1	0.618	1.98	3.21	3.09	22.74
EQ+20%CH_4	40.0%	40.0%	20.0%	-	-	100.0%	1	0.622	2.00	3.21	3.80	26.58
EQ+10%CO_2	45.0%	45.0%	-	10.0%	-	90.0%	1	0.733	2.35	3.21	2.14	14.22
EQ+20%CO_2	40.0%	40.0%	-	20.0%	-	80.0%	1	0.851	2.73	3.21	1.90	10.88
EQ+10%N_2	45.0%	45.0%	-	-	10.0%	90.0%	1	0.667	2.14	3.21	2.14	15.62
EQ+20%N_2	40.0%	40.0%	-	-	20.0%	80.0%	1	0.720	2.31	3.21	1.90	12.86
Bamboo	19.7%	21.0%	1.5%	11.9%	45.9%	42.2%	0.94	1.070	3.43	3.21	1.11	5.22
Rubber wood	17.6%	20.4%	1.4%	10.8%	49.8%	39.4%	0.86	1.020	3.27	3.21	1.00	4.80
Wood pellets	21.7%	20.8%	2.2%	12.6%	42.7%	44.7%	1.04	0.987	3.17	3.21	1.22	5.79
Rice husk	19.8%	22.6%	2.0%	13.1%	42.5%	44.4%	0.88	1.01	3.24	3.21	1.20	5.57

*The fuel compositions of producer gas of bamboo, rubber wood, wood pellets, and rich husk are researched by [2], [3], [28], [29], and [30].

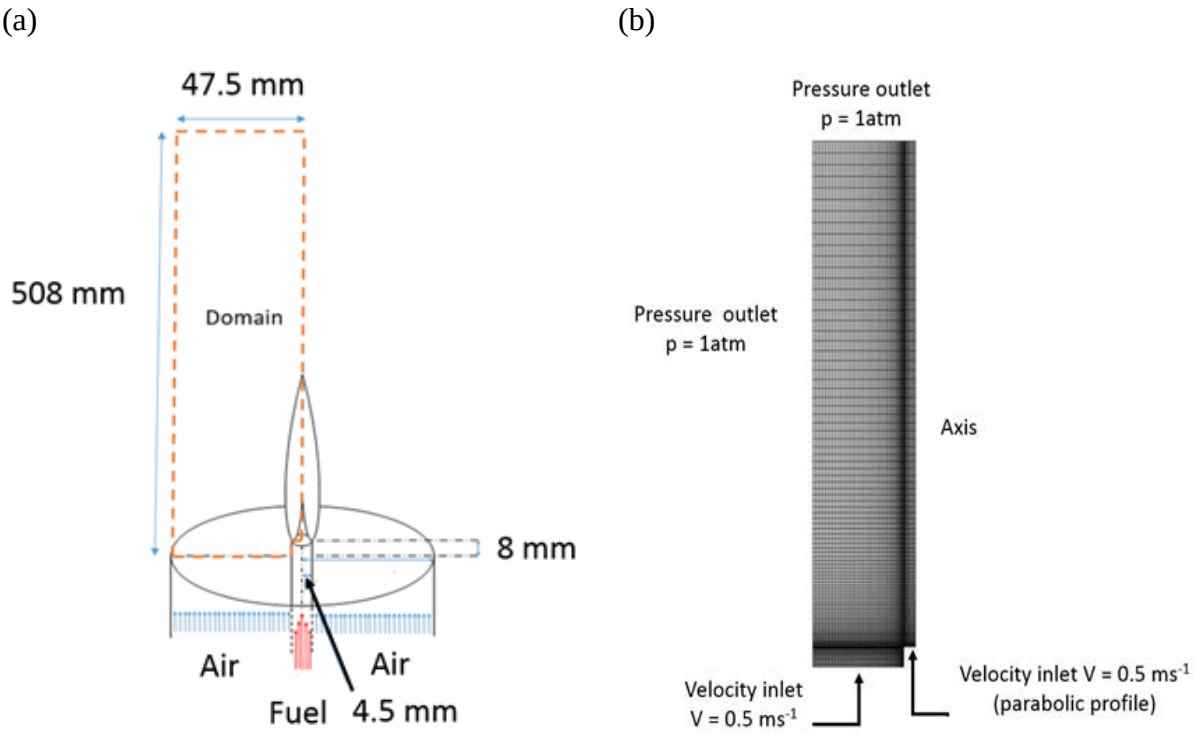

Figure 1 Left: Physical appearance, dimension of the burner, and volume of interest. Right: Generated mesh and boundary conditions

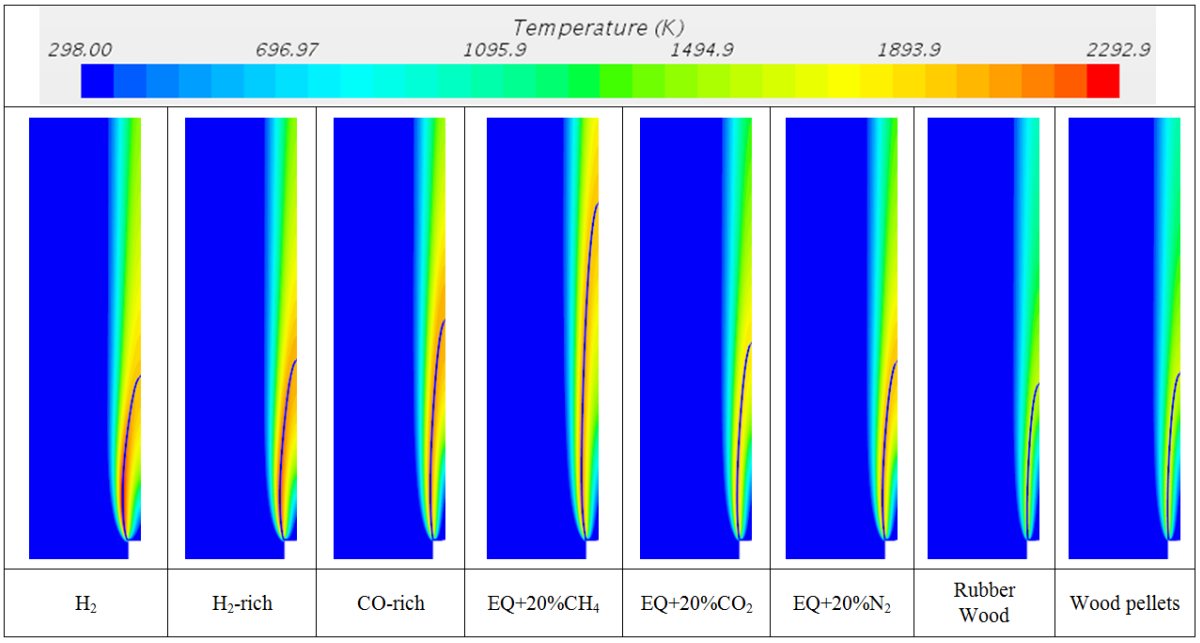

Figure 2 Temperature contour

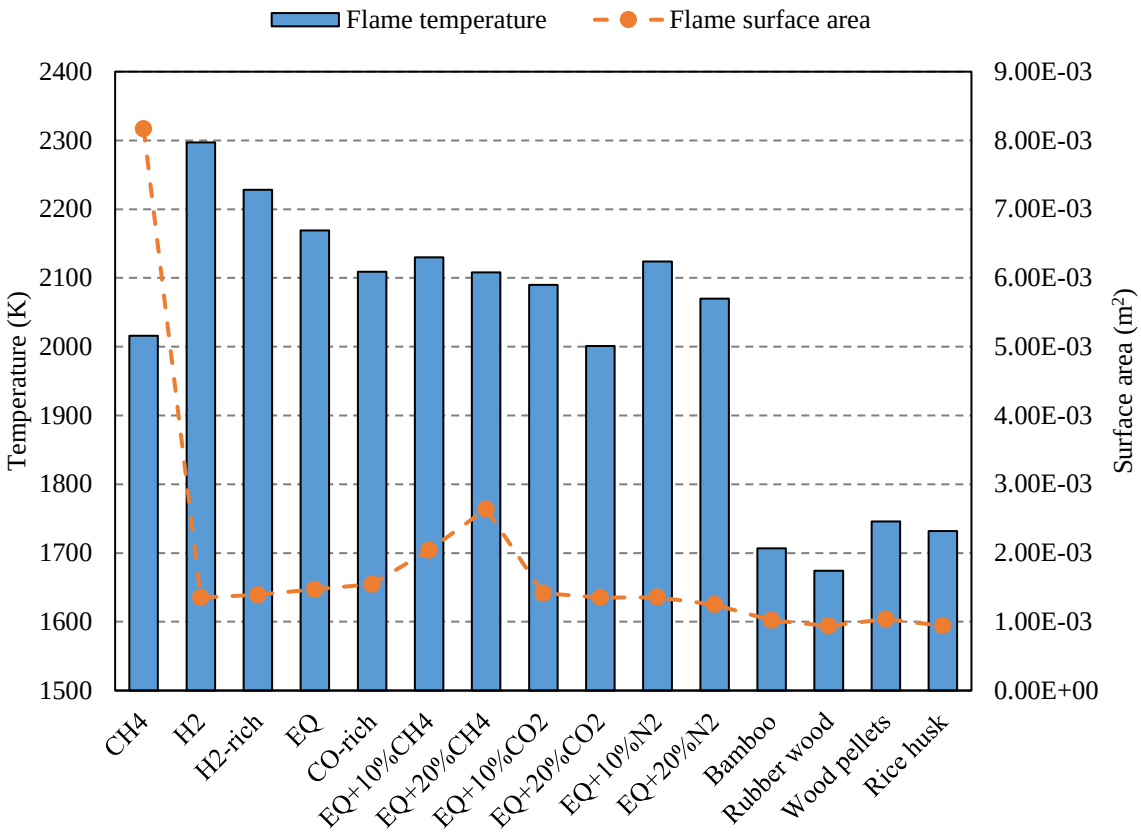

Figure 3 Flame temperature (T) and surface area (A_f)

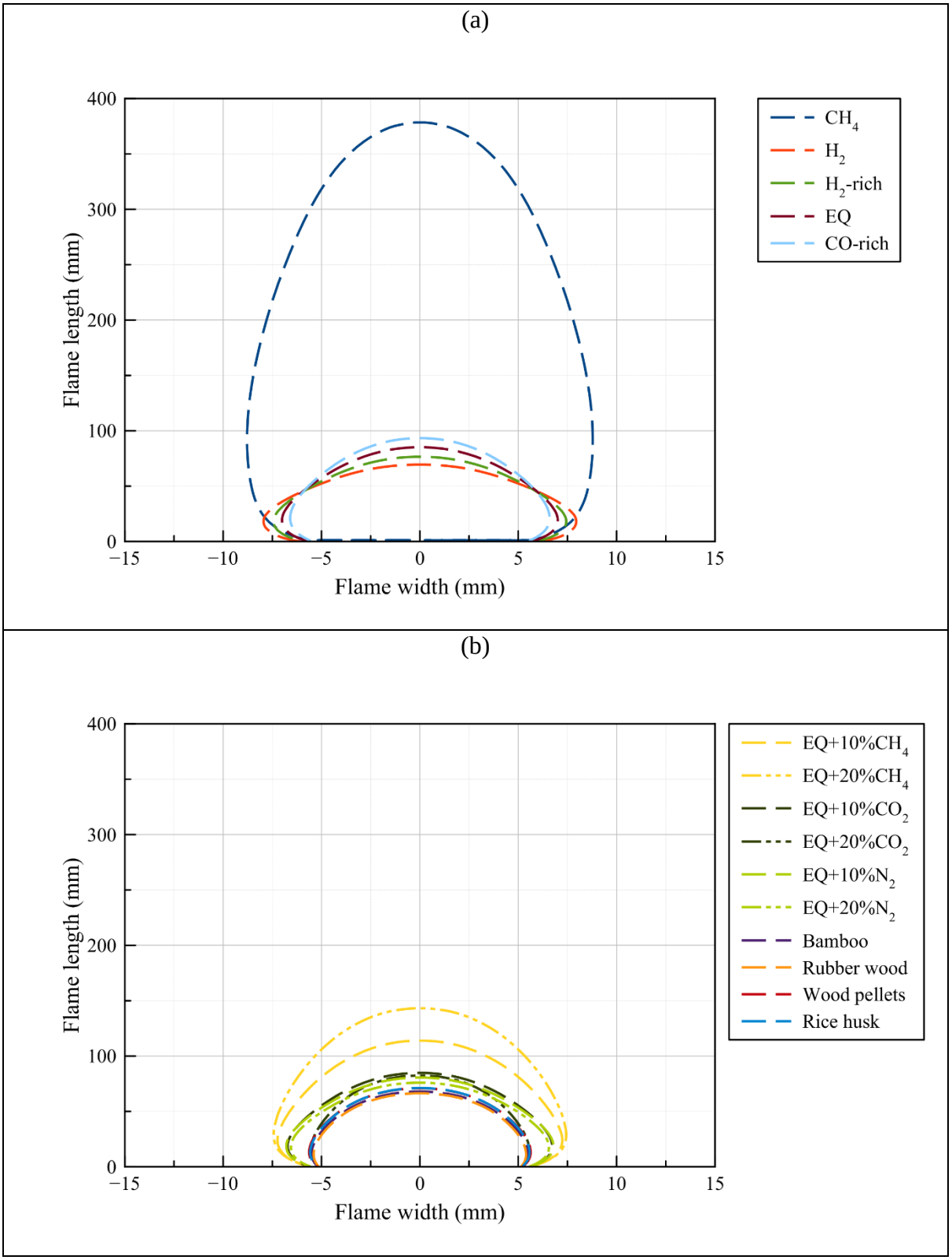

Figure 4 Flame front line of (a) H_2, CH_4, and syngas, and (b) syngas mixed with CH_4, CO_2, and N_2, and producer gas

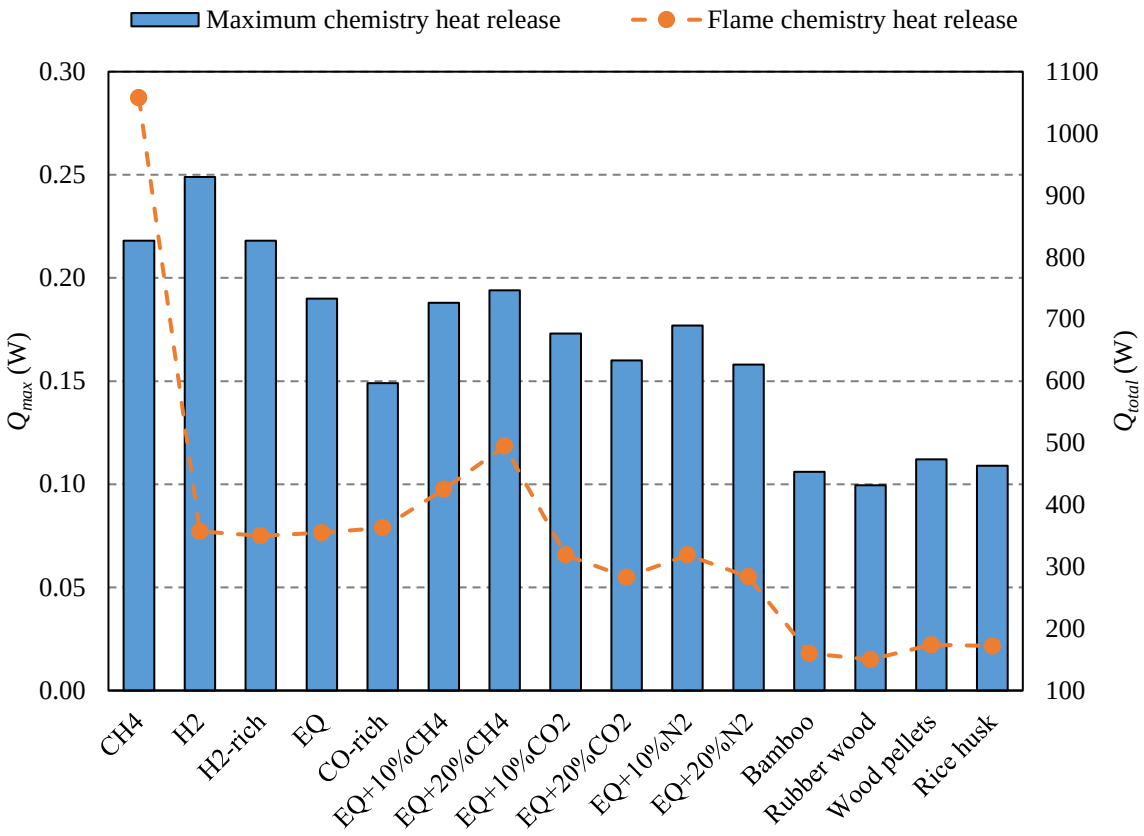

Figure 5 Maximum chemistry heat release (Q_{max}) and Flame chemistry heat release (Q_{tatal})

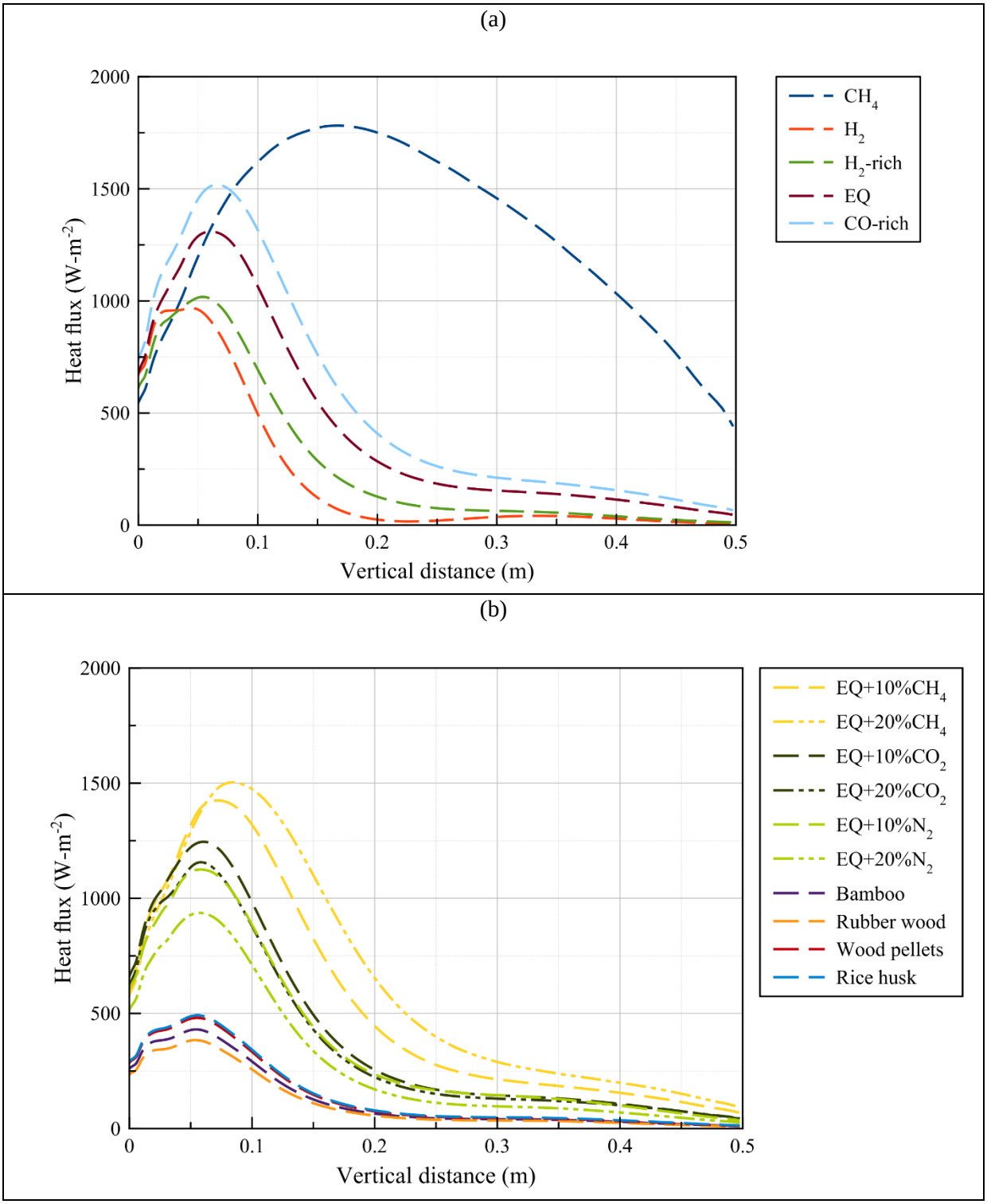

Figure 6 Heat flux profile on the outlet boundary (a) H_2, CH_4, and syngas (b) syngas mixed with CH_4, CO_2, and N_2 and producer gas of different feed stocks

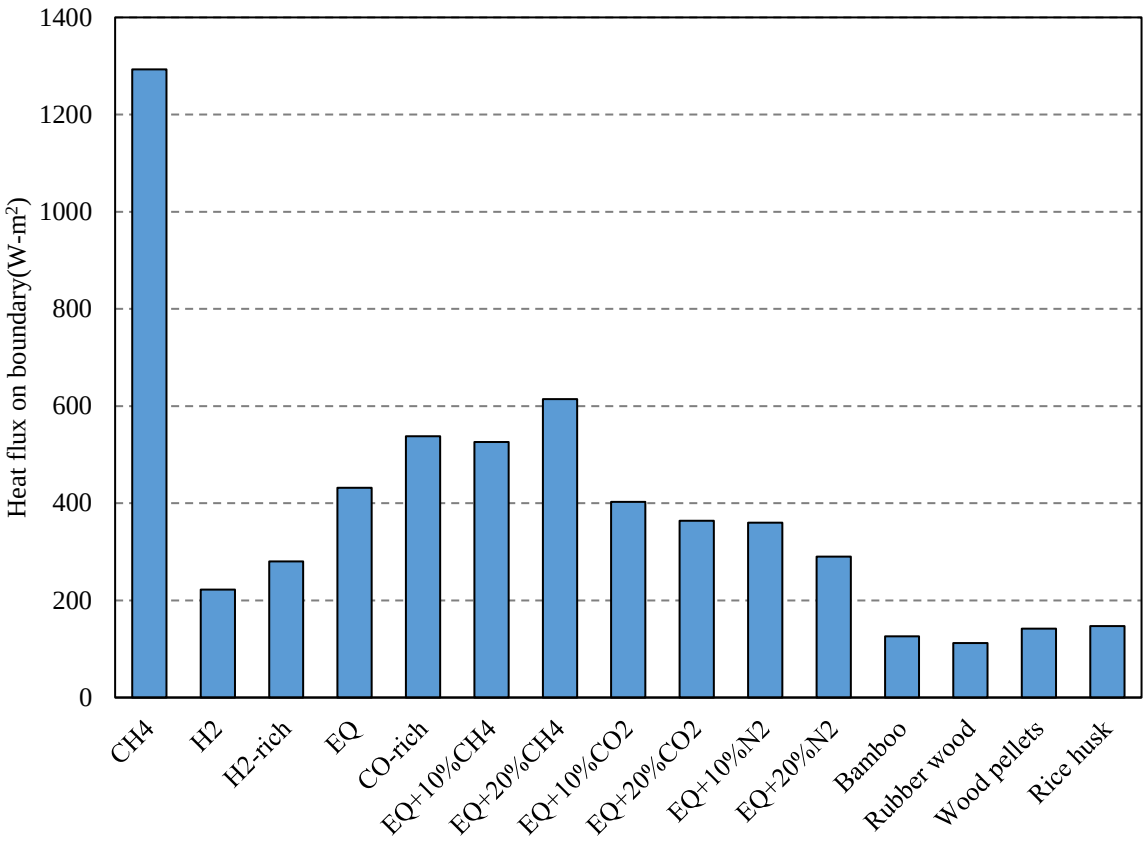

Figure 7 Average heat flux on measured boundary

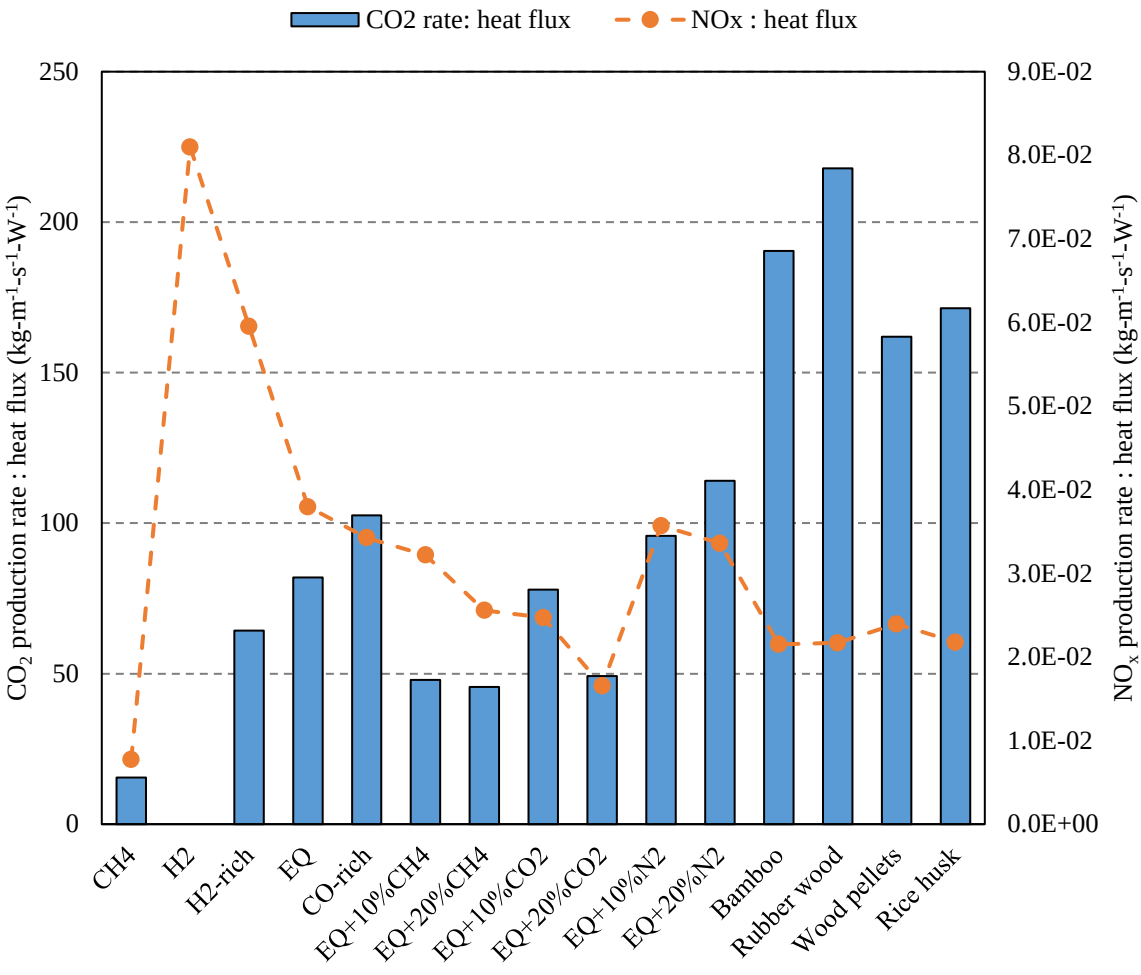

Figure 8 Emission production rate of CO_2 and NO_x per generated heat flux